Parental Allele-Specific Protein Synthesis Dynamics in Single Cells *In Vivo*

Chiu-An Lo[1], Brian E. Chen[1,2,*]

[1] Centre for Research in Neuroscience, Research Institute of the McGill University Health Centre, Montréal, Québec, Canada.

[2] Departments of Medicine and Neurology & Neurosurgery, McGill University, Montréal, Québec, Canada.

*Correspondence to: brian.chen@mcgill.ca

Abstract

Proteins are synthesized based on the changing availability of ribosomes, and the rates of protein synthesis control the growth and functions of cells. But how the dynamics of protein synthesis vary across cells in an animal is not known. Here, we measure the dynamics of protein synthesis of the Ribosomal protein L13a (Rpl13a) from both parental alleles simultaneously in single cells in the living animal. We use genome-edited *Drosophila* that have a quantitative reporter of protein synthesis inserted into the endogenous *Rpl13a* locus. We find that protein synthesis burst frequencies and durations from each parental allele were similar among cells within a tissue, but not across tissues. We identify the histone methyltransferase EHMT to be required for the inheritance of protein synthesis dynamics among the cells within each tissue. Our results demonstrate that protein synthesis rates are tissue-specific and regulated by epigenetic modification.

One sentence summary

Epigenetic modification sets protein synthesis rates across each tissue.

Highlights

1. We used genome editing to insert a quantifiable protein translation reporter into the endogenous *Ribosomal protein L13a* gene and thus track the protein synthesis of both parental alleles simultaneously in every single cell in the awake animal.
2. We find that protein synthesis is bursty even between the two parental alleles, and cells from the same tissue have similar protein synthesis dynamics, indicating a common origin for rates of synthesis, set by a progenitor cell. This is the first time that translational bursting in an animal has been shown.
3. Cells can preferentially express one parental allele over the other, and this varies across tissues and over time, and also occurs in cell clusters.
4. The histone methyltransferase EHMT controls the similarity of protein synthesis dynamics within a tissue, and other histone modifiers do not.

Introduction

Protein synthesis is the limiting step in generating the final molecular outcome of DNA. Messenger RNAs wait for free ribosomes to translate the message into proteins, with higher rates of protein synthesis enabling a cell to have faster growth and more functions. However, it has not been possible to measure protein synthesis dynamics in multicellular organisms. Thus, in order to track and quantify the dynamics of protein synthesis in single cells in animals, we used the Protein Quantitation Ratioing (PQR) technique (**Figure 1A**) (Lo et al. 2015). Using CRISPR-Cas9 genome editing of *Drosophila melanogaster*, we inserted a *PQR* DNA construct with a red fluorescent protein (RFP) reporter at the end of the coding sequence for the *Ribosomal protein L13a* (*Rpl13a*) gene (Lo et al. 2015) (**Figure 1A**). This animal produces one molecule of RFP for every one molecule of Rpl13a protein that is made during protein synthesis. Therefore, the red fluorescence intensity in a cell is proportional to the Rpl13a concentration and can be used to track and measure Rpl13a dynamics over time in every cell in the animal. We chose Rpl13a because, as a ribosomal subunit, it is itself involved in protein translation and has a long turnover rate similar to fluorescent proteins (Mazumder et al. 2003; Chaudhuri et al. 2007; Kapasi et al. 2007; Boisvert et al. 2012; Jia et al. 2012; Lo et al. 2015). Rpl13a is expressed in all cells at moderately high levels with several hundreds of mRNA copies per cell (Lo et al. 2015). *Rpl13a* mRNA expression dynamics in the brain and in the whole organism are not circadian driven in flies and mice (Keegan et al. 2007; Hughes et al. 2010; Hughes et al. 2012). Rpl13a is also frequently used as a control "housekeeping" gene in quantitative DNA measurements because of its resistance to external effects and stability (Mane et al. 2008).

Results

Measuring protein synthesis dynamics in single cells in the awake animal

Inserting *PQR-RFP* into the endogenous *Rpl13a* locus resulted in an entirely red fluorescent animal (**Figure 1B**). These *Drosophila* were easily identified by their strong red fluorescence everywhere, which increased globally as the animal developed (**Figure 1B**). Although individual cells were not distinguishable in these animals, we used these animals to verify that global Rpl13a is arrhythmic over hourly timescales. To distinguish individual cells, we created two more genome-edited *Drosophila* PQR lines that sequestered RFP or blue fluorescent protein (BFP) into the nucleus, Rpl13a-PQR-RFP_{nols} and Rpl13a-PQR-BFP_{nols} animals, respectively (**Figure 1B**). Nuclear localization signals tend to result in fluorescent proteins leaking into the cytosol. We added a nucleolar localization signal (Tsai et al. 2008) to RFP (RFP_{nols}) and BFP (BFP_{nols}) because nucleolar localized fluorescent proteins spread only into the nucleus (Lo et al. 2015).

In single cell organisms gene expression is a stochastic process due to the low copy number of DNA, RNA, and ribosome molecules (Fraser et al. 2004; Kaern et al. 2005; Yu et al. 2006; Raj and van Oudenaarden 2008; Salari et al. 2012; Vogel and Marcotte 2012; Guimaraes et al. 2014; Dar et al. 2015), but it has not been possible to examine these questions in animals. We wanted to know whether the expression of a gene with high mRNA levels would still occur in stochastic bursts or whether it would exhibit a sustained expression. We tracked endogenous Rpl13a protein production in single cells *in vivo* by measuring red and blue fluorescence intensities in the nucleus over time scales of seconds to days (**Methods**). To avoid the effects of anesthesia on protein translation, we imaged awake animals immobilized using a suction microfluidics chamber (Mishra et al. 2014). Images were acquired at varying time intervals to verify that the time course of fluorescence signals were not due to changes in animal positioning, movement, imaging depth, photobleaching, or changes in the nucleus and nucleolus (**Figure 1C,**

Methods). Imaging every 2, 4, or 5 minutes for 5 hours, we observed bursts of protein translation over timescales of tens of minutes in both the Rpl13a-PQR-RFP_{nols} and Rpl13a-PQR-BFP_{nols} animals (**Figure 1C**). Interestingly, we observed that cells from within the same tissue were more likely to have similar protein expression dynamics than between tissues (**Figure 1C**), demonstrating that protein dynamics are regulated in each tissue. On average, a single cell would produce 4.2 ± 1.9 protein synthesis events every 30 minutes (mean ± S.D., n = 209 cells, 7 animals), but there was considerable heterogeneity between single cells and between individual animals (**Figure 1D**). To determine the temporal spread of the protein translation events, we performed an autocorrelation analysis on the fluorescence time course from single cells (Yu et al. 2006). A single exponential decay fit to the autocorrelation function gave an average time constant of $\tau = 8.5 \pm 8.1$ minutes as an unbiased estimate of protein synthesis burst duration (mean ± S.D., n = 142 cells, 7 animals; **Figure 1E; Methods**). At this stage, nearly all cells in larvae are fully differentiated and are simply growing rapidly in size without dividing (Smith and Orr-Weaver 1991). Despite these accelerated metabolic and growth demands of the larva, ribosomal protein expression is not constitutive but occurs in bursts.

Individual cells can have remarkably biased protein expression for one allele

Mothers produce the oocyte and contribute to it nutrients, proteins, and mRNA molecules, until zygotic expression of both the maternal and paternal genes turn on. What percentage of cells express both the mother's and father's allele at any given time? We sought to examine the dynamics of protein expression between each of the parent-of-origin *Rpl13a* alleles after zygotic expression turns on. We took advantage of the two colors of the PQR lines and crossed them to create transheterozygous *Rpl13a-PQR-RFP_{nols}* / *Rpl13a-PQR-BFP_{nols}* animals,

from Rpl13a-PQR-RFP$_{nols}$ mothers and Rpl13a-PQR-BFP$_{nols}$ fathers, or vice versa (**Figure 2**), to track expression of each allele. We verified that oocytes from Rpl13a-PQR-RFP$_{nols}$ mothers had only red (i.e., maternal expression) within cells (**Figure 2A**), until the dark period when all maternal expression is degraded during the maternal to zygotic transition (Tadros and Lipshitz 2005; Schier 2007; Baroux et al. 2008). Upon zygotic (i.e., genomic) expression of Rpl13a protein, we found that both parental alleles were expressed at the same time across the organism (**Figure 2A**). Imaging transheterozygous larvae at different days, we found that 100% of cells had both red and blue nuclei, as might be expected for a gene expressed at fairly high levels. The majority of cells had similar fluorescence intensities of RFP and BFP (**Figure 2A**). First, we wanted to verify that there were equivalent levels of mRNA between the parental alleles which might roughly correlate to equivalent levels of red and blue fluorescence, even though we and others have shown that mRNA amounts correlate poorly with protein quantity, including for Rpl13a (Schwanhausser et al. 2011; Vogel and Marcotte 2012; Lo et al. 2015). We performed qPCR on single cells isolated from transheterozygous *Rpl13a-PQR-RFP$_{nols}$* / *Rpl13a-PQR-BFP$_{nols}$* animals and found 941 ± 1066 mRNA molecules from the maternal allele and 943 ± 878 mRNA molecules from the paternal allele (n = 53 cells, 32 animals, 12 from PQR-RFP$_{nols}$ fathers). These results show that the broadly similar levels of red versus blue fluorescence intensities across the animal do correspond with broadly similar levels of mRNA expression from the respective alleles. Thus, by adjusting the fluorescence imaging acquisition to be equivalent values between red and blue fluorescence for most cells in the animal, we sought to measure the relative differences between the paternal versus maternal Rpl13a protein expression in individual cells. Using the ratio between the red to blue PQR fluorescence expression in each nucleus, we measured the distribution of relative contributions of each parental allele in cells in

the proventriculus, gut, salivary gland, fat body, trachea, and epidermis. Most cells expressed both alleles relatively equally, but we frequently observed biases for one parental allele over the other within multiple clusters of cells in a single animal (*n* = 17 animals, 7 from PQR-RFPnols fathers and 10 from PQR-BFPnols fathers, **Figure 2B**). However, we never observed a complete silencing or systematic bias across the animal for an allele (Wang et al. 2008; Gregg et al. 2010a; Gregg et al. 2010b; DeVeale et al. 2012; Xie et al. 2012; Crowley et al. 2015). Some cells express very little of one allele leading to differences as large as 64-fold between the two alleles (**Figure 2B**). Thus, it is important to note that each parental allele in an animal will not necessarily be evenly expressed at the protein level in all cells.

Does a heterozygous animal express half as much RNA or protein as a homozygous animal? Our single cell qPCR results show that not every cell expresses an equal amount of each parental allele, and this is also the case at the protein level, with some cells barely expressing an allele (**Figure 2B**). In other words, if the choice to express either parental allele is stochastic, and the correlation between RNA and protein is poor, then many cells in a heterozygous animal will not necessarily be heterozygous at the RNA nor protein levels. We sought to visualize this relationship between DNA to RNA to protein distributions (**Figure 2C**). We isolated 79 single cells from 24 transheterozygous Rpl13a-PQR-RFPnols / Rpl13a-PQR-BFPnols animals and 88 cells from 14 homozygous Rpl13a-PQR-RFPnols animals and then measured their PQR fluorescence intensities before performing single cell qPCR. The linear correlation between *Rpl13a* mRNA and protein expression was weak, with coefficients of determination, R^2 values close to 0. However, the average number of *RFP* mRNA in single cells in the heterozygotes was 979 ± 776 compared to 1650 ± 1241 in the homozygotes. The RFP fluorescence intensity per heterozygous cell was 338 ± 209 compared to 738 ± 484 in the homozygotes. Thus, even with

stochastic mechanisms governing the DNA transcription of either allele, RNA expression amounts, and protein synthesis, a large number of cells in an organism averages out the noise to produce more protein from two copies of DNA versus a single copy of the allele.

Protein synthesis dynamics are more similar for cells in the same tissue

After *Drosophila* embryos hatch as larvae, they enter a period of rapid cell growth where mitosis ceases and cells expand in size. Once the protein synthesis dynamics are set in the progenitor cells, do the differentiated larval cells within each tissue maintain similar dynamics over time? To measure the protein expression dynamics of both parental alleles, we imaged transheterozygous *Rpl13a-PQR-RFP*$_{nols}$ / *Rpl13a-PQR-BFP*$_{nols}$ awake animals every 15 minutes over time periods of 5 hours (n = 8 animals, 4 from PQR-RFP$_{nols}$ fathers; **Figure 3A**–**C**). Cross-correlation analysis between the fluorescence time courses of each cell within a tissue showed that each tissue had its own degree of similarity in synthesis dynamics amongst its constituent cells (**Figure 3D**, **E**). For example, epidermal cells had a high degree of cross-correlation of their protein synthesis time signatures (**Figure 3F**), which was significantly different than the intra-tissue cross-correlation values of salivary gland (t-test $t(579) = 13.4$, $p < 0.001$, $n = 20$ cells) and proventriculus ($t(1208) = 34.8$, $p < 0.001$, $n = 25$ cells, compared to $n = 30$ epidermal cells). Cross-correlations of synthesis dynamics between cells across different tissues were significantly weaker than the protein synthesis dynamics within a tissue (epidermis versus salivary gland $t(1077) = 8.9$, $p < 0.001$ and epidermis versus proventriculus $t(1527) = 19.4$, $p < 0.001$, **Figure 3F)**. This was not due to the local cellular environment or local imaging conditions, but from cells being derived from a common progenitor, as cells that were farther than 50 µm apart but from the same tissue were more likely to be correlated than those from

different tissues ($t(660) = 13.42$, $p < 0.001$, 343 intra-tissue comparisons and 331 inter-tissue comparisons).

Allele-specific biases in protein dynamics change over time

Does a cell maintain its ratio of parental allele expression over time? Tracking the ratio of expression between the paternal and maternal Rpl13a allele over time from 144 cells revealed that most cells did not show more than a 4-fold bias for either parental allele (**Figure 3G**). The average paternal/maternal ratios in single cells over time from different tissues were 1.186 ± 0.858 (epidermis), 1.044 ± 0.709 (salivary gland), and 0.960 ± 0.419 (proventriculus) (mean ± S.D., n = 5 animals, 3 from PQR-RFP_{nols} fathers). Thus, over time the majority of cells express close to equal amounts between the two parental alleles, but still many cells will express a > 4-fold difference between the two alleles (**Figure 2B, 3G**). Interestingly, this bias can invert, as we found that 21% of cells that expressed a > 2-fold difference between the parental alleles would invert their allele preference ratio to a > 2-fold bias for the other allele (**Figure 3G**). This emphasizes the dynamic nature of allelic expression and shows that the heterozygosity of a single cell can dramatically change over time.

EHMT controls the similarity of protein synthesis dynamics within a tissue

During tissue development, progenitor cells must respond to an animal's changing environment and pass on these molecular decisions to their cellular descendants, such as an appropriate concentration of ribosomes. This is predominantly achieved through heritable epigenetic marks acting on the physical DNA strands. We sought to identify histone modifiers that might regulate the inheritance of protein synthesis dynamics across sister cells. Using

specific small-molecule inhibitors of histone lysine methyltransferases, we identified UNC0638 as a potent disruptor of the cross-correlation of protein synthesis dynamics between cells within a tissue (< 25% of the cross-correlation values overlap between wild-type and UNC0638-fed animals, **Figure 4A–F**). UNC0638 specifically inhibits the histone H3 lysine 9 methyltransferase activity of euchromatic histone-lysine N-methyltransferase (EHMT/GLP). To determine whether EHMT might control *Rpl13a* RNA expression, we performed qPCR on single cells isolated from $EHMT^{null}$ mutants compared to $EHMT^{+}$ control (precise excision). We found that $EHMT^{null}$ mutants had lower levels of *Rpl13a* mRNA (5012 ± 2609, n = 16 cells, 2 animals) compared to controls (8463 ± 5524, n = 17 cells, 2 animals), indicating that methylation of lysine 9 on histone 3 might coordinate protein synthesis. To verify the specificity of the EHMT histone modification on inheritance of protein synthesis dynamics, we used two *EHMT* null mutants $EHMT^{DD1}$; ; *Rpl13a-PQR-RFP*$_{nols}$ / *Rpl13a-PQR-BFP*$_{nols}$ and $EHMT^{DD2}$; ; *Rpl13a-PQR-RFP*$_{nols}$ / *Rpl13a-PQR-BFP*$_{nols}$ (Kramer et al. 2011). We found that loss of function EHMT reduced the cross-correlations of protein synthesis dynamics between cells within the epidermis (n = 51 cells, 2 wild-type animals; n = 19 cells, 1 *EHMT* null animal), salivary gland (n = 20 cells, 1 wild-type animal; n = 40 cells, 2 *EHMT* null animals), and proventriculus (n = 24 cells, 1 wild-type animal; n = 65 cells, 3 *EHMT* null animals), with < 25% of the cross-correlation values overlapping between wild-type and *EHMT* null animals (**Figure 4G–L**). These results were specific for this histone H3 modification, as the histone H3 lysine 27 demethylase mutant *UTX* (Copur and Muller 2013) had a broad overlap of cross-correlation values compared to wild-type (**Supplemental Figure S1**). These results demonstrate that EHMT alters ribosomal gene expression dynamics to heritably control protein synthesis rates. Histone methylation may be

one mechanism by which ribosomal availability can be regulated and inherited by daughter cells across a tissue.

Discussion

We used fluorescent proteins to report the protein synthesis dynamics of Rpl13a. After protein synthesis of Rpl13a and the PQR fluorescent protein reporter, both proteins must fold and mature to function. It is not known how long the Rpl13a protein takes to function after its synthesis, but it is similar in size to the red and blue fluorescent proteins used in our experiments, which we estimate to take one hour to fluoresce after synthesis at 25°C (Balleza et al. 2018). Therefore, we focused our analysis on the synthesis events rather than quantifying amounts of functional Rpl13a. That is, we quantified protein synthesis burst events, and their duration until protein synthesis paused, as a readout for ribosomal protein synthesis dynamics. The time required for fluorescence does not allow for immediate detection of the protein synthesis event, but this lag time only results in a delay and an increased variability in quantifying the events. However, our protein synthesis burst measurements are in agreement with previous measurements in single cell organisms (Yu et al. 2006). Instantaneous detection of protein synthesis events would provide more accurate burst duration and burst frequency measurements.

By measuring the protein synthesis dynamics of multiple tissues in the same animal, we found a smaller variance in dynamics within an animal than the variance from the same tissue across different animals. Although these results argue that protein synthesis rates are set by early common progenitor cells, it remains to be seen whether these rates eventually change over time as the animal ages and the different tissue requirements and functions exert more control over ribosomal availabilities. During embryonic development, histone modifications inherited from

progenitor cells can regulate the expression of ribosomal genes to control translation dynamics. Eventually the dilution of these modified nucleosomes that occurs with each cell division will loosen this regulatory grip (Laprell et al. 2017). Once cell proliferation ceases at the larval stage, any remaining epigenetic control that exists among sister cells might be fixed or may weaken over time. Precise temporal control in removing histone modifications, in addition to finer tools to manipulate histone modifications, will help reveal the functions of these inherited marks.

Although protein activity is the ultimate executor of gene expression, RNA levels are frequently used as a proxy, and so knowing the correlation between a gene's mRNA and protein products is important to many biologists. For example, up to half of proteins with circadian rhythms do not have rhythmic mRNAs (Reddy et al. 2006; Robles et al. 2014). Protein abundance is critically important in some genes, where the loss of expression of one copy of the gene can cause diseases and disorders collectively called haploinsufficiencies. Our results examining allelic expression at the RNA and protein levels demonstrate that heterozygous and homozygous definitions vary from cell to cell and over time. This asymmetry can allow a disease mutation in one of the parental alleles to be solely expressed during DNA replication, or spatially in a section of a neuron's dendrite. Overall within a tissue, the protein expression between two alleles balances out (**Figure 2B**), but still, close to 50% of cells in an animal can have a > 2-fold difference between the two alleles. Furthermore, these biases can change over time in single cells (**Figure 3G**), further highlighting the fluid definition of allelic expression. Despite the noise in mRNA and protein production, the underlying structure that is set by the integer copy numbers of DNA (i.e., one allele expression versus two allele expression) is clear and detectable with even a moderate number of cells (**Figure 2C**). These cellular and temporal

differences in allelic expression have important consequences for understanding diseases caused by haploinsufficiency and copy number variations.

Experimental Procedures

Preparation of sgRNA Expression vectors

Different single guide RNAs (sgRNAs) were designed in a 20 base pair DNA oligonucleotide format to guide the Cas9 nuclease to the end of the coding region of *Drosophila Rpl13a*. They were optimized using the on-line Optimal Target Finder algorithm (http://tools.flycrispr.molbio.wisc.edu/targetFinder). Individual sgRNAs were synthesized and cloned into the backbone of the *pCFD3: U6:3-gRNA* vector (Addgene #49410) (Port et al. 2014). Each sgRNAs was co-transfected along with a Cas9 expressing plasmid, pBS-Hsp70-Cas9 (Addgene #46294), and a circular *Rpl13a* repair template into cultured *Drosophila S2* cells using TransIT Insect Transfection Reagent (Mirus Bio LLC, Madison, WI, USA). Gene editing efficiency of the different sgRNAs was evaluated five days after transfection by cellular fluorescence and genotyping using a primer outside of the homology arm and the other inside the inserted *PQR* sequence.

Construction of *PQR* Repair Template

The genomic sequences of *Drosophila Ribosomal protein L13A* were identified using GeneDig (https://genedig.org) (Suciu et al. 2015) and then PCR amplified from Canton-S fly genomic DNA lysates to construct the 5' and 3' homology arms of 1.4 kilobase each. The 5' homology arm did not include the endogenous *Rpl13a* promoter, to prevent the expression of the transgene until the in-frame genomic integration at the correct locus. The three different *Protein Quantitation Reporters* with a fluorescent protein with and without a nucleolar localization

signal were inserted between the 5' and 3' homology arms to generate three different *Rpl13a*-specific repair templates as described (Lo et al. 2015).

Generation of sgRNA-expressing transgenic fly

The optimal sgRNA in *pCFD3: U6:3-gRNA* vector was microinjected into embryos (BestGene, Inc) to create a transgenic fly constitutively expressing the *Rpl13a*-specific sgRNA. This sgRNA fly was then crossed to a *nos-Cas9* fly (*yw*; *attP40 {nos-Cas9}/CyO*) to restrict CRISPR-Cas9 activity to minimize lethality (Port et al. 2014). Circular *Rpl13a* repair template was then microinjected into the embryos containing both active Cas9 and sgRNA (BestGene, Inc). Surviving flies were intercrossed with one another and the resulting offspring were screened for red or blue fluorescence signals at wandering 3rd instar larval stage. RFP or BFP positive larvae were collected and out-crossed to the Canton-S strain to remove the Cas9 and sgRNA genes. The integrated *PQR-RFP*, *PQR-RFP$_{nols}$*, or *PQR-BFP$_{nols}$* at the *Rpl13a* locus at the 3rd chromosome was balanced by crossing to a TM3 balancer line. All of three genome-edited fly lines (Rpl13a-PQR-RFP, Rpl13a-PQR-RFP$_{nols}$ and Rpl13a-PQR-BFP$_{nols}$) were verified by genotyping and sequencing.

Fly husbandry

Flies of different genotypes were reared in a 25°C humidity controlled incubator with a 12:12 hour light/dark cycle. Embryos were collected for 4 hours (stage 12-16) on apple juice agar plates and the hatched larvae were imaged at the next day or 2 or 3 days later. Homozygous and transheterozygous embryos or larvae were collected for imaging. Oocytes from

transheterozygous females were used to confirm maternal expression of Rpl13a, which was expressed strongly, but then decreased rapidly in embryos.

EHMT null (*EHMT*^{DD1}; ; *Rpl13a-PQR-RFP*$_{nols}$ / *Rpl13a-PQR-BFP*$_{nols}$ and *EHMT*^{DD2} ; ; *Rpl13a-PQR-RFP*$_{nols}$ / *Rpl13a-PQR-BFP*$_{nols}$) larvae were obtained by crossing *w; ; Rpl13a-PQR-RFP*$_{nols}$*/TM3* to *EHMT*^{null} imprecise p-element excision flies (gifts from Dr. Annette Schenck). The control EHMT fly line used was the precise excision of the same genetic background (Kramer et al. 2011). Larvae were used at 3 days old for experiments. UNC0638 containing apple agar plates were used to collect embryos and used for the larvae food source. These larvae were used at 3 days old for experiments.

Quantitative Real-Time PCR

Single cell imaging and subsequent qPCR was performed as previously described (Lo et al. 2015). Individual cells were imaged in drops of culture media on Teflon-coated glass slides before extraction and purification of total RNA using the TRIzol reagent (Life Technologies). Total RNA was reverse-transcribed with gene-specific primers (2µM final concentration) using Superscript III reverse-polymerase (Life Technologies). This cDNA template was used for real-time PCR using the TaqMan Fast Advanced Mastermix (Life Technologies). Real-time PCR amplification was detected using the StepOnePlus Real-Time PCR System (Applied Biosystems) and cycle quantification values were calculated using the StepOne software. Experiments were performed in two to three experimental replicates with two technical replicates. Absolute quantification was determined using standard curves generated with synthesized oligo standards containing the *Rpl13a* target. Primers specific for *Rpl13a-PQR-RFP* and *Rpl13a-PQR-BFP* were less efficient (86%) than primers for wildtype *Rpl13a*, which can result in less accurate

absolute RNA quantifications. Primers and double-quenched 5'-FAM/ZEN/IowaBlackFQ-3' probes were purchased from Integrated DNA Technologies (Coralville, IA).

Image Acquisition

Fluorescence images were taken using an Olympus laser scanning confocal microscope FV1000 at 800 x 800 pixels with a 20× or 40× oil objective, N.A. 0.85 and 1.30 corresponding to a 636 x 636 µm and 317 x 317 µm field of view, respectively, or a custom built 2-photon laser scanning microscope at 512 x 512 pixels with a 40× water objective, 1.0 N.A. corresponding to an approximately 310 x 310 µm field of view. Fluorescence emission was detected by photomultiplier tubes. All image acquisition parameters were fixed during imaging sessions for excitation intensity, exposure time, gain, and voltages. Animals were imaged at late stage embryos (>16 hours after egg laying), and three different developmental stages (1, 2, and 3 days after hatching) of the transparent larvae. For long term time-lapse imaging, larvae were immobilized and accommodated in a microfluidic chamber (larva chip) over the course of imaging (Mishra et al. 2014). Larvae were coated with Halocarbon 700 oil to avoid dehydration. Images were acquired between every 60 seconds to every 15 minutes for 3 to 7 hours total duration.

Image Analysis

Average fluorescence pixel intensities were measured in one region of interest (of 2 x 2, 4 x 4, or 5 x 5 pixels for epidermal, fat body, or gut cells, respectively) that covered 70% of the nuclei using ImageJ as described (Lo et al. 2015). Fluorescence pixel intensities were background subtracted and presented in arbitrary units. No bleed-through was detected between

red and blue fluorescence channels. Images in figures were adjusted for contrast and brightness for presentation. To verify that changes in fluorescence intensity over time were not due to changes in nucleolar and nucleus size and shape, we imaged Rpl13a-PQR-RFP animals where the RFP fluorescence is within the cytosol (**Figure 1B**). In initial experiments we crossed Rpl13a-PQR-RFP with Rpl13a-PQR-BFP_{nols} animals to use the blue nucleus as a marker for individual cells, but the RFP was found to dimerize with the BFP and accumulate in the nucleus, as we have observed previously in mammalian cells. In Rpl13a-PQR-RFP animals, we analyzed cytoplasmic RFP fluorescence dynamics in putative single cells using one region of interest of 6 x 6 pixels. Analysis of protein synthesis burst frequency and duration was not significantly different from animals with fluorescence contained within the nucleus, with an average time constant of $\tau = 8.3 \pm 7.8$ minutes from cytoplasmic fluorescence (mean ± S.D., $n = 36$ cells, 3 animals) compared to 8.5 ± 8.1 minutes from the nuclear fluorescence.

Statistical Analysis

Autocorrelation and cross-correlation analyses (Yu et al. 2006) were performed using custom-written programs in MatLab (MathWorks, Natick, MA). Protein translation events were defined as any increase in fluorescence from the immediately preceding time point. All statistical analyses were performed using custom-written programs in MatLab.

Acknowledgments

The authors thank Ibrahim Kays, Farida Emran, Júnia Vieira dos Santos, Isabela Fabri Karam, Leah Dawson, and ChenHui Zhao for assistance with experiments and analysis. This work was supported by grants (to B.E.C.) from the Natural Sciences and Engineering Research Council of Canada, and the Canadian Institutes of Health Research (148882).

Author Contributions

B.E.C. designed the experiments and supervised the project. C.L. and B.E.C. performed experiments and analyzed the data. C.L. and B.E.C. wrote the manuscript.

No competing financial interests to declare.

Correspondence and requests for materials should be addressed to brian.chen@mcgill.ca

Supplemental Information is provided as one supplemental figure.

Figures and Figure Legends

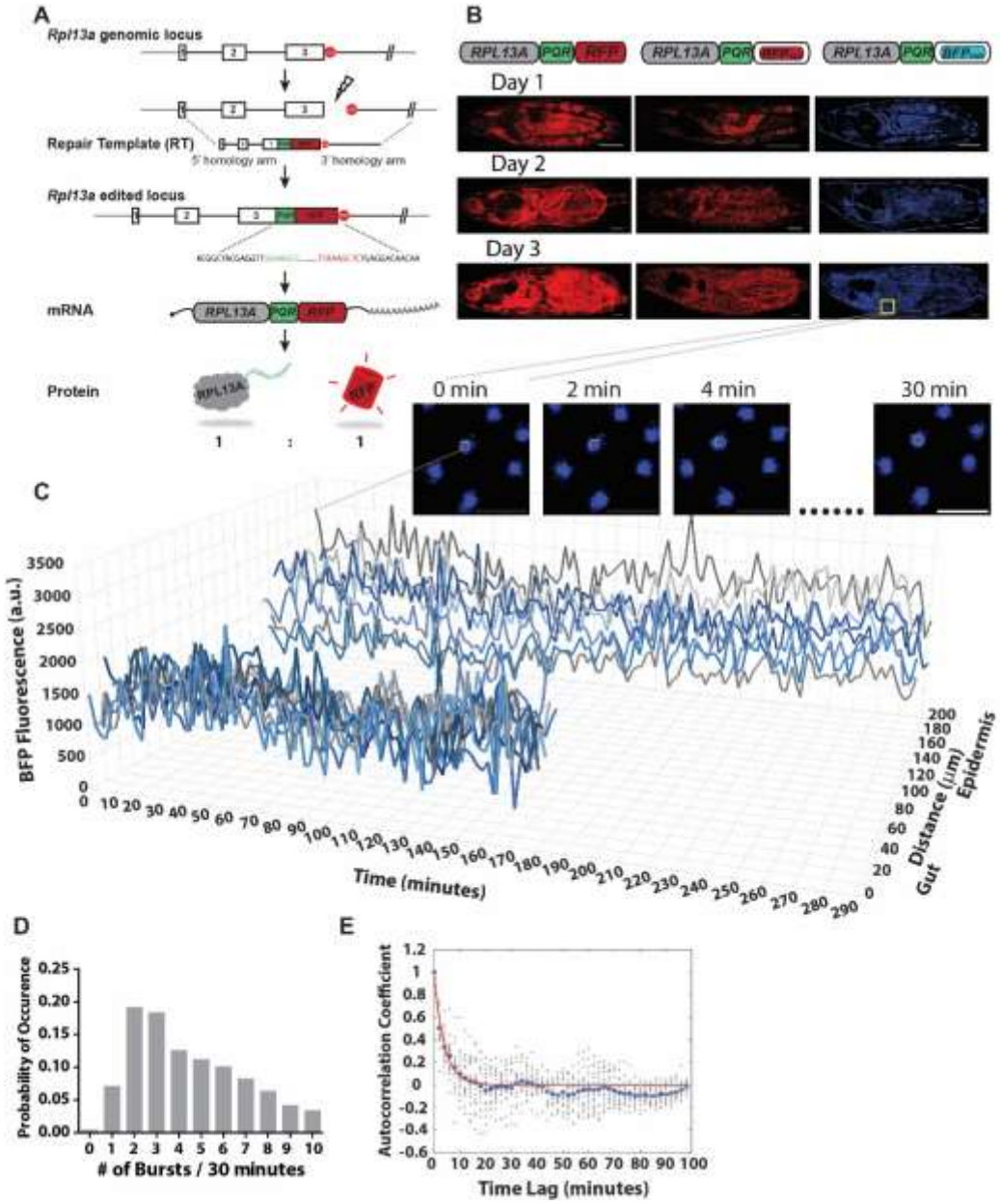

Figure 1, Quantification of Rpl13a protein production in single cells in the living animal.

(A) Insertion of a *Protein Quantitation Reporter* (*PQR*) into the endogenous *Rpl13a* gene can quantify protein amounts. The *PQR* is inserted before the final stop codon using CRISPR-Cas9 genome editing (lightning bolt). The break is repaired using homologous recombination of an exogenous repair template containing the *PQR* and appropriate homology arms. Colored nucleotide sequences represent genomic sequencing results of a *PQR-RFP* insertion into

Drosophila melanogaster. During protein synthesis the *PQR* produces a stoichiometric ratio of red fluorescent protein (RFP) and Rpl13a protein.

(B) Rpl13a increases expression across the animal over days. Three different lines of genome-edited *Drosophila melanogaster* were created, Rpl13a-PQR-RFP, Rpl13a-PQR-RFP_{nols} and Rpl13a-PQR-BFP_{nols}. A nucleolar localization signal was used to sequester the RFP or blue fluorescent protein into the nucleus (RFP_{nols} or BFP_{nols}, respectively) to visualize individual cells. Fluorescence intensity in each nucleus is used to measure Rpl13a production over time (inset). Scale bars, 100 µm (main images), 10 µm (inset).

(C) Rpl13a protein expression dynamics occur on timescales of tens of minutes. Homozygous Rpl13a-PQR-BFP_{nols} larvae were restrained and imaged every 2 minutes for 5 hours. Neighboring cells in each tissue had similar protein synthesis dynamics. Blue fluorescence intensities from 8 cells in the epidermis and 10 cells from the gut are shown.

(D) Protein synthesis occurs in stochastic bursts over tens of minutes. The frequency distribution of protein translation bursts per 30 minutes (**D**) had an average of 4.2, but with large variance among cells (S.D. = 1.9).

(E) Autocorrelation analysis of the single cell fluorescence time course provided an unbiased estimate of the temporal variation in protein translation events. Single exponential fits (representative trace in red) to the autocorrelation function from individual epidermal cells in a single animal produced an average $\tau = 9.8 \pm 6.5$ minutes. The average burst duration across all cells and animals was 8.5 ± 8.1 minutes.

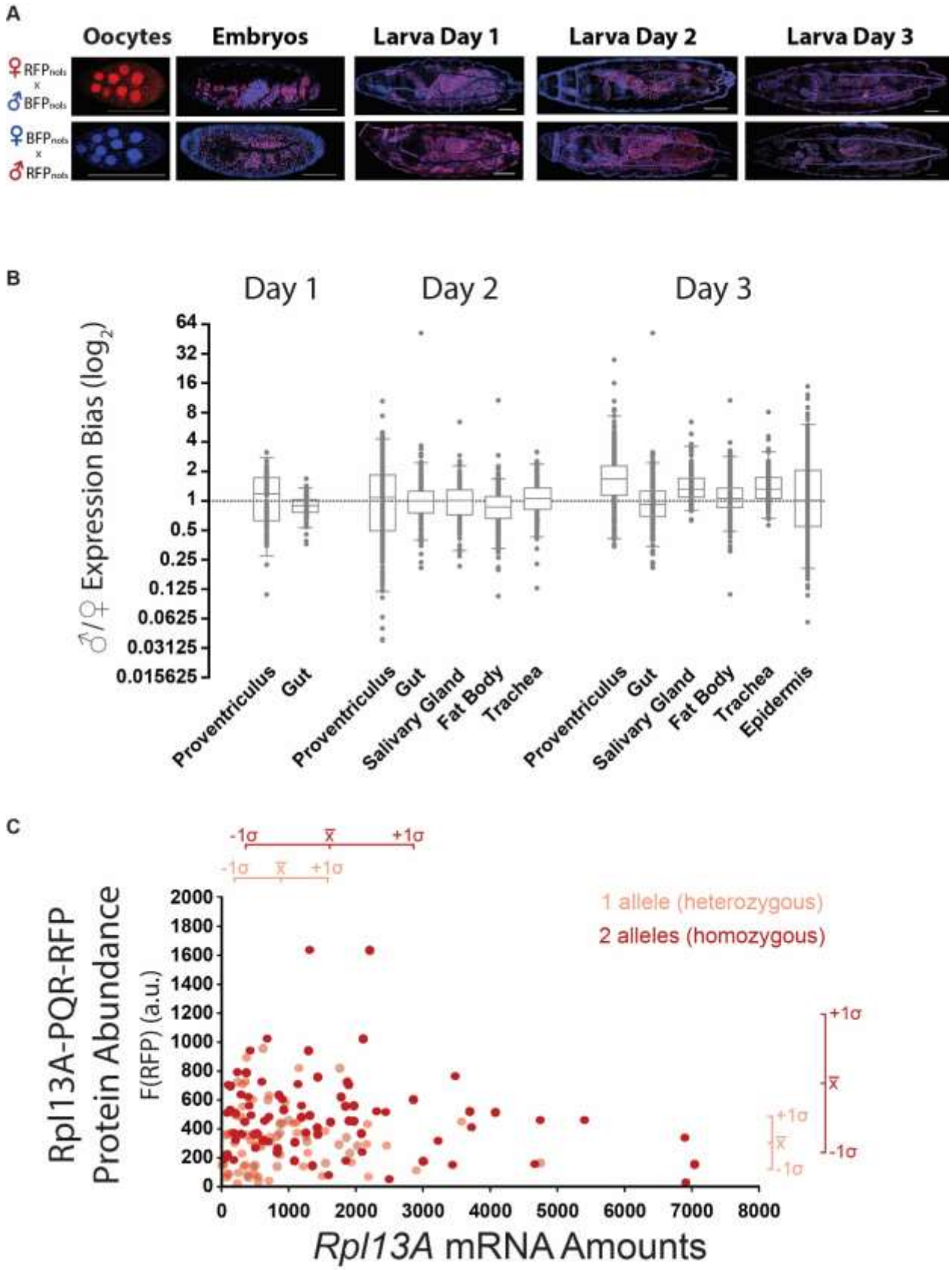
A
Oocytes
Embryos
Larva Day 1
Larva Day 2
Larva Day 3
B
Day 1
Day 2
Day 3
♂/♀ Expression Bias (log2)
64
32
16
8
4
2
1
0.5
0.25
0.125
0.0625
0.03125
0.015625
Proventriculus
Gut
Salivary Gland
Fat Body
Trachea
Epidermis
C
Rpl13A-PQR-RFP Protein Abundance
F(RFP) (a.u.)
1 allele (heterozygous)
2 alleles (homozygous)
-1σ
x̄
+1σ
0
200
400
600
800
1000
1200
1400
1600
1800
2000
0
1000
2000
3000
4000
5000
6000
7000
8000
Rpl13A mRNA Amounts

Figure 2, Clusters of cells within a tissue have a biased expression for a parental allele.

(A) Rpl13a-PQR-RFP_{nols} and Rpl13a-PQR-BFP_{nols} parents produced transheterozygous progeny whose specific parent-of-origin Rpl13a allele can be tracked using color. Maternal expression of Rpl13a was only detected in oocytes, where it is expressed at high levels and then decreases rapidly in embryos. Rpl13a expression is only detectable again in late embryos, simultaneously from both the maternal and paternal alleles. Most cells express both alleles equally, relative to the blue and red fluorescence intensities, but clusters of cells within the same tissue had similar allelic biases. Scale bars, 100 µm.

(B) The ratio of the paternal to maternal Rpl13a protein expression was measured in single cells across different tissues and from both combinations of Rpl13a-PQR-RFP_{nols} and Rpl13a-PQR-BFP_{nols} parents. Box plots represent the median and 1st and 3rd quartiles of the data and error bars are 2.5 and 97.5 percentiles.

(C) The relationships between DNA allele number, RNA, and protein numbers. Single cells were isolated from heterozygous and homozygous Rpl13a-PQR-RFP_{nols} animals and their fluorescence intensities and mRNA amounts were measured. Despite the weak correlation between mRNA and protein levels, the difference between having one copy of DNA expressed versus having two copies of the allele is evident from the population data. Even stochastically, homozygous animals are able to reach mRNA and protein levels greater than a single allele is, with higher values 1 standard deviation greater than the mean ($\bar{x}+1\sigma$) in homozygotes than in heterozygotes.

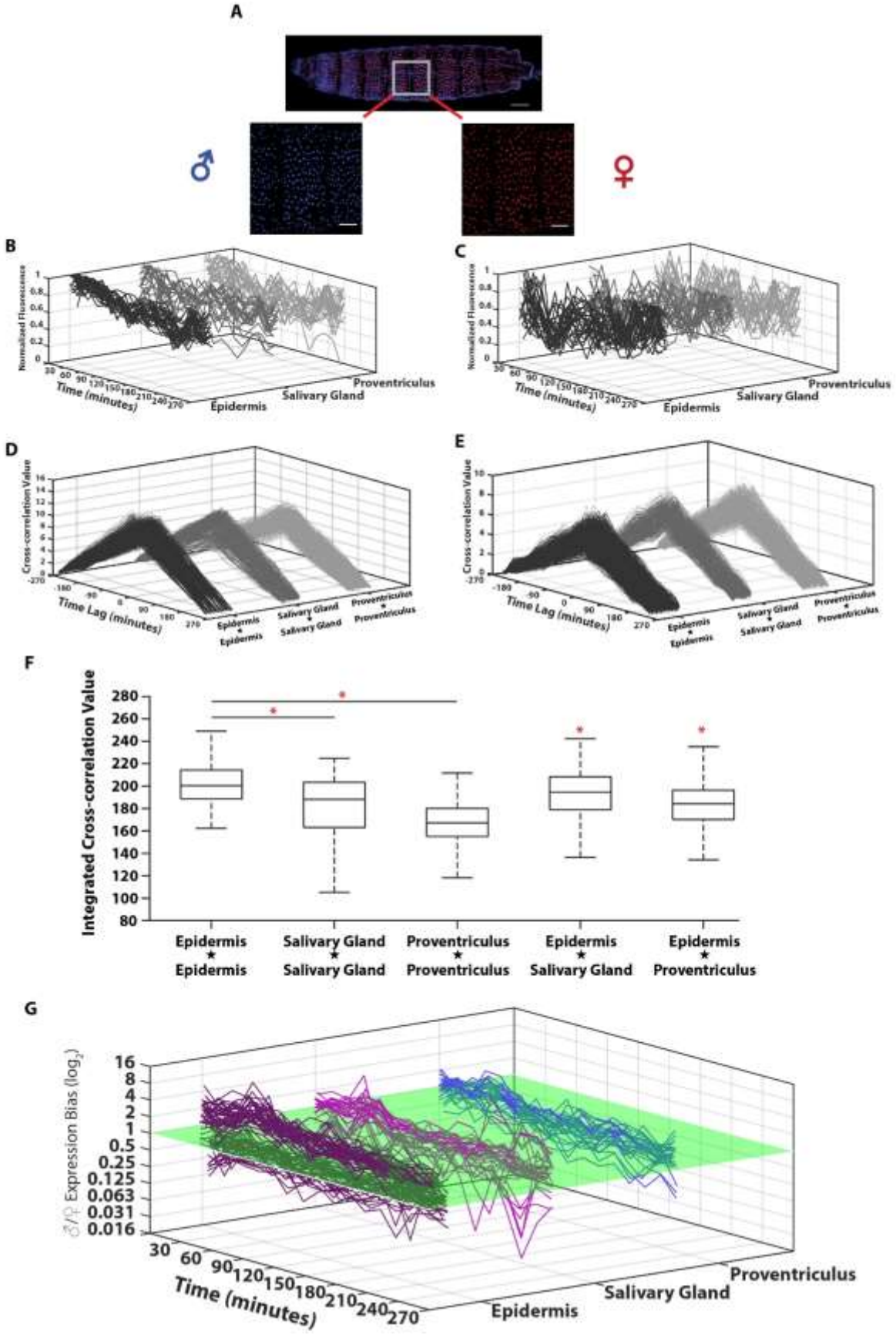
A
♂
♀
B
Normalized Fluorescence
Time (minutes)
Epidermis
Salivary Gland
Proventriculus
C
Normalized Fluorescence
Time (minutes)
Epidermis
Salivary Gland
Proventriculus
D
Cross-correlation Value
Time Lag (minutes)
Epidermis * Epidermis
Salivary Gland * Salivary Gland
Proventriculus * Proventriculus
E
Cross-correlation Value
Time Lag (minutes)
Epidermis * Epidermis
Salivary Gland * Salivary Gland
Proventriculus * Proventriculus
F
Integrated Cross-correlation Value
Epidermis * Epidermis
Salivary Gland * Salivary Gland
Proventriculus * Proventriculus
Epidermis * Salivary Gland
Epidermis * Proventriculus
G
♂/♀ Expression Bias (log2)
Time (minutes)
Epidermis
Salivary Gland
Proventriculus

Figure 3, Parental allele-specific protein expression over time shows regulation and randomness.

(A–C) Each parent-of-origin allele of Rpl13a can be tracked and quantified in Rpl13a-PQR-RFP_{nols}/Rpl13a-PQR-BFP_{nols} transheterozygous animals using the blue and red fluorescence intensities of the cell nucleus (**A**). Protein synthesis dynamics from paternal (**B**) and maternal (**C**) alleles from each cell in different tissues were measured at 15-minute intervals. Scale bars, 100 µm in whole animal image, 50 µm in magnified images.

(D, E) Cross-correlation analysis of the protein synthesis time course between two cells was performed to examine the degree of similarity of the protein expression dynamics. Each pairwise cross-correlation between cells within three tissues (epidermis, salivary gland, or proventriculus) is shown.

(F) Integrated cross-correlation values show the overall similarity of protein synthesis dynamics among the constituent cells of each tissue. Epidermal cells had higher degrees of cross-correlation than salivary gland or proventricular cells ($p < 0.001$). Cross-correlation analysis of the protein synthesis dynamics between two cells from different tissues showed a significant decrease in similarity compared to intra-tissue correlations ($p < 0.001$), showing that cells of the same origin have more similar protein synthesis dynamics. Box plots represent the median and 1st and 3rd quartiles of the data and error bars are the range.

(G) The ratio of paternal to maternal allele expression changes over time. Each curve represents the fluorescence ratio from an individual cell. The surface plane denotes equal expression of paternal and maternal alleles. Curves crossing the surface plane represent an inversion of allele preference expression at the time. The majority of cells maintain close to equal expression of each allele over timescales of hours. However, at any given time many cells will express a > 2-fold expression preference for one parental allele, and even this bias can invert over time.

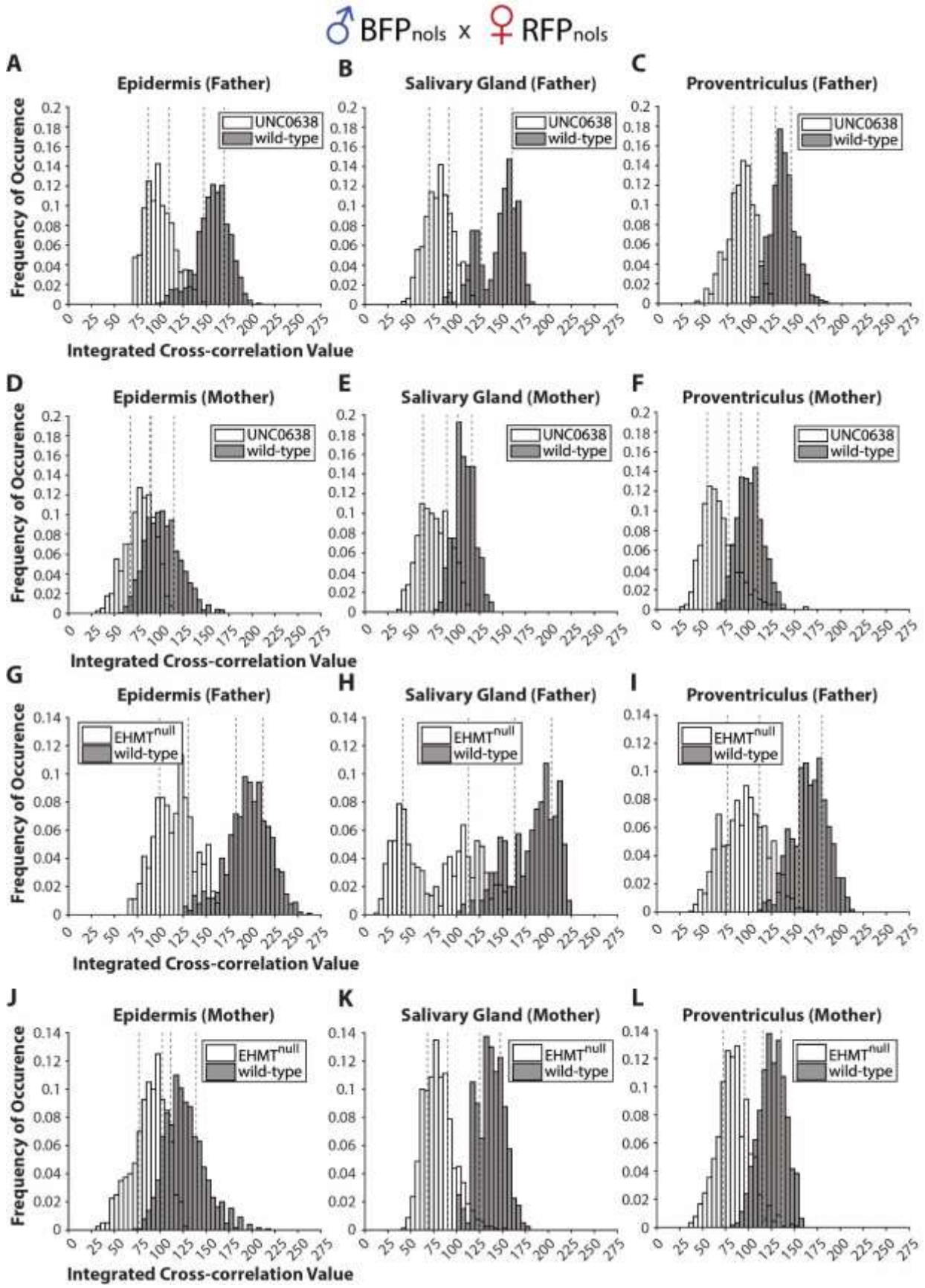
♂ BFPnols x ♀ RFPnols
A
Epidermis (Father)
B
Salivary Gland (Father)
C
Proventriculus (Father)
D
Epidermis (Mother)
E
Salivary Gland (Mother)
F
Proventriculus (Mother)
G
Epidermis (Father)
H
Salivary Gland (Father)
I
Proventriculus (Father)
J
Epidermis (Mother)
K
Salivary Gland (Mother)
L
Proventriculus (Mother)
UNC0638
wild-type
EHMTnull
wild-type
Frequency of Occurence
Integrated Cross-correlation Value

Figure 4, EHMT is required to maintain correlated protein synthesis dynamics among cells within a tissue.

(A–F) The EHMT enzyme inhibitor UNC0638 decreases the correlation in protein synthesis dynamics between cells within a tissue. Dashed grey lines denote 1st and 3rd quartiles in the distribution of integrated cross-correlation values.

(G–L) Loss of function EHMT animals have decreased correlation between cells of their protein synthesis dynamics. Thus, the heritable activity of the EHMT histone methyltransferase is required to maintain the correlated protein synthesis rates found across each tissue.

References

Balleza E, Kim JM, Cluzel P. 2018. Systematic characterization of maturation time of fluorescent proteins in living cells. *Nat Methods* **15**: 47-51.

Baroux C, Autran D, Gillmor CS, Grimanelli D, Grossniklaus U. 2008. The maternal to zygotic transition in animals and plants. *Cold Spring Harb Symp Quant Biol* **73**: 89-100.

Boisvert FM, Ahmad Y, Gierlinski M, Charriere F, Lamont D, Scott M, Barton G, Lamond AI. 2012. A quantitative spatial proteomics analysis of proteome turnover in human cells. *Mol Cell Proteomics* **11**: M111 011429.

Chaudhuri S, Vyas K, Kapasi P, Komar AA, Dinman JD, Barik S, Mazumder B. 2007. Human ribosomal protein L13a is dispensable for canonical ribosome function but indispensable for efficient rRNA methylation. *RNA* **13**: 2224-2237.

Copur O, Muller J. 2013. The histone H3-K27 demethylase Utx regulates HOX gene expression in Drosophila in a temporally restricted manner. *Development* **140**: 3478-3485.

Crowley JJ, Zhabotynsky V, Sun W, Huang S, Pakatci IK, Kim Y, Wang JR, Morgan AP, Calaway JD, Aylor DL et al. 2015. Analyses of allele-specific gene expression in highly divergent mouse crosses identifies pervasive allelic imbalance. *Nat Genet* **47**: 353-360.

Dar RD, Razooky BS, Weinberger LS, Cox CD, Simpson ML. 2015. The Low Noise Limit in Gene Expression. *PloS one* **10**: e0140969.

DeVeale B, van der Kooy D, Babak T. 2012. Critical evaluation of imprinted gene expression by RNA-Seq: a new perspective. *PLoS Genet* **8**: e1002600.

Fraser HB, Hirsh AE, Giaever G, Kumm J, Eisen MB. 2004. Noise minimization in eukaryotic gene expression. *PLoS Biol* **2**: e137.

Gregg C, Zhang J, Butler JE, Haig D, Dulac C. 2010a. Sex-specific parent-of-origin allelic expression in the mouse brain. *Science* **329**: 682-685.

Gregg C, Zhang J, Weissbourd B, Luo S, Schroth GP, Haig D, Dulac C. 2010b. High-resolution analysis of parent-of-origin allelic expression in the mouse brain. *Science* **329**: 643-648.

Guimaraes JC, Rocha M, Arkin AP. 2014. Transcript level and sequence determinants of protein abundance and noise in Escherichia coli. *Nucleic Acids Res* **42**: 4791-4799.

Hughes ME, Grant GR, Paquin C, Qian J, Nitabach MN. 2012. Deep sequencing the circadian and diurnal transcriptome of Drosophila brain. *Genome Res* **22**: 1266-1281.

Hughes ME, Hogenesch JB, Kornacker K. 2010. JTK_CYCLE: an efficient nonparametric algorithm for detecting rhythmic components in genome-scale data sets. *J Biol Rhythms* **25**: 372-380.

Jia J, Arif A, Willard B, Smith JD, Stuehr DJ, Hazen SL, Fox PL. 2012. Protection of extraribosomal RPL13a by GAPDH and dysregulation by S-nitrosylation. *Mol Cell* **47**: 656-663.

Kaern M, Elston TC, Blake WJ, Collins JJ. 2005. Stochasticity in gene expression: from theories to phenotypes. *Nat Rev Genet* **6**: 451-464.

Kapasi P, Chaudhuri S, Vyas K, Baus D, Komar AA, Fox PL, Merrick WC, Mazumder B. 2007. L13a blocks 48S assembly: role of a general initiation factor in mRNA-specific translational control. *Mol Cell* **25**: 113-126.

Keegan KP, Pradhan S, Wang JP, Allada R. 2007. Meta-analysis of Drosophila circadian microarray studies identifies a novel set of rhythmically expressed genes. *PLoS Comput Biol* **3**: e208.

Kramer JM, Kochinke K, Oortveld MA, Marks H, Kramer D, de Jong EK, Asztalos Z, Westwood JT, Stunnenberg HG, Sokolowski MB et al. 2011. Epigenetic regulation of learning and memory by Drosophila EHMT/G9a. *PLoS Biol* **9**: e1000569.

Laprell F, Finkl K, Muller J. 2017. Propagation of Polycomb-repressed chromatin requires sequence-specific recruitment to DNA. *Science* **356**: 85-88.

Lo C-A, Kays I, Emran F, Lin T-J, Cvetkovska V, Chen Brian E. 2015. Quantification of Protein Levels in Single Living Cells. *Cell Reports* **13**: 2634-2644.

Mane VP, Heuer MA, Hillyer P, Navarro MB, Rabin RL. 2008. Systematic method for determining an ideal housekeeping gene for real-time PCR analysis. *Journal of biomolecular techniques : JBT* **19**: 342-347.

Mazumder B, Sampath P, Seshadri V, Maitra RK, DiCorleto PE, Fox PL. 2003. Regulated release of L13a from the 60S ribosomal subunit as a mechanism of transcript-specific translational control. *Cell* **115**: 187-198.

Mishra B, Ghannad-Rezaie M, Li J, Wang X, Hao Y, Ye B, Chronis N, Collins CA. 2014. Using microfluidics chips for live imaging and study of injury responses in Drosophila larvae. *J Vis Exp*: e50998.

Port F, Chen HM, Lee T, Bullock SL. 2014. Optimized CRISPR/Cas tools for efficient germline and somatic genome engineering in Drosophila. *Proceedings of the National Academy of Sciences of the United States of America* **111**: E2967-2976.

Raj A, van Oudenaarden A. 2008. Nature, nurture, or chance: stochastic gene expression and its consequences. *Cell* **135**: 216-226.

Reddy AB, Karp NA, Maywood ES, Sage EA, Deery M, O'Neill JS, Wong GK, Chesham J, Odell M, Lilley KS et al. 2006. Circadian orchestration of the hepatic proteome. *Curr Biol* **16**: 1107-1115.

Robles MS, Cox J, Mann M. 2014. In-vivo quantitative proteomics reveals a key contribution of post-transcriptional mechanisms to the circadian regulation of liver metabolism. *PLoS Genet* **10**: e1004047.

Salari R, Wojtowicz D, Zheng J, Levens D, Pilpel Y, Przytycka TM. 2012. Teasing apart translational and transcriptional components of stochastic variations in eukaryotic gene expression. *PLoS Comput Biol* **8**: e1002644.

Schier AF. 2007. The maternal-zygotic transition: death and birth of RNAs. *Science* **316**: 406-407.

Schwanhausser B, Busse D, Li N, Dittmar G, Schuchhardt J, Wolf J, Chen W, Selbach M. 2011. Global quantification of mammalian gene expression control. *Nature* **473**: 337-342.

Smith AV, Orr-Weaver TL. 1991. The regulation of the cell cycle during Drosophila embryogenesis: the transition to polyteny. *Development* **112**: 997-1008.

Suciu RM, Aydin E, Chen BE. 2015. GeneDig: a web application for accessing genomic and bioinformatics knowledge. *BMC Bioinformatics* **16**: 67.

Tadros W, Lipshitz HD. 2005. Setting the stage for development: mRNA translation and stability during oocyte maturation and egg activation in Drosophila. *Dev Dyn* **232**: 593-608.

Tsai KW, Tseng HC, Lin WC. 2008. Two wobble-splicing events affect ING4 protein subnuclear localization and degradation. *Experimental cell research* **314**: 3130-3141.

Vogel C, Marcotte EM. 2012. Insights into the regulation of protein abundance from proteomic and transcriptomic analyses. *Nat Rev Genet* **13**: 227-232.

Wang X, Sun Q, McGrath SD, Mardis ER, Soloway PD, Clark AG. 2008. Transcriptome-wide identification of novel imprinted genes in neonatal mouse brain. *PloS one* **3**: e3839.

Xie W, Barr CL, Kim A, Yue F, Lee AY, Eubanks J, Dempster EL, Ren B. 2012. Base-resolution analyses of sequence and parent-of-origin dependent DNA methylation in the mouse genome. *Cell* **148**: 816-831.

Yu J, Xiao J, Ren X, Lao K, Xie XS. 2006. Probing gene expression in live cells, one protein molecule at a time. *Science* **311**: 1600-1603.

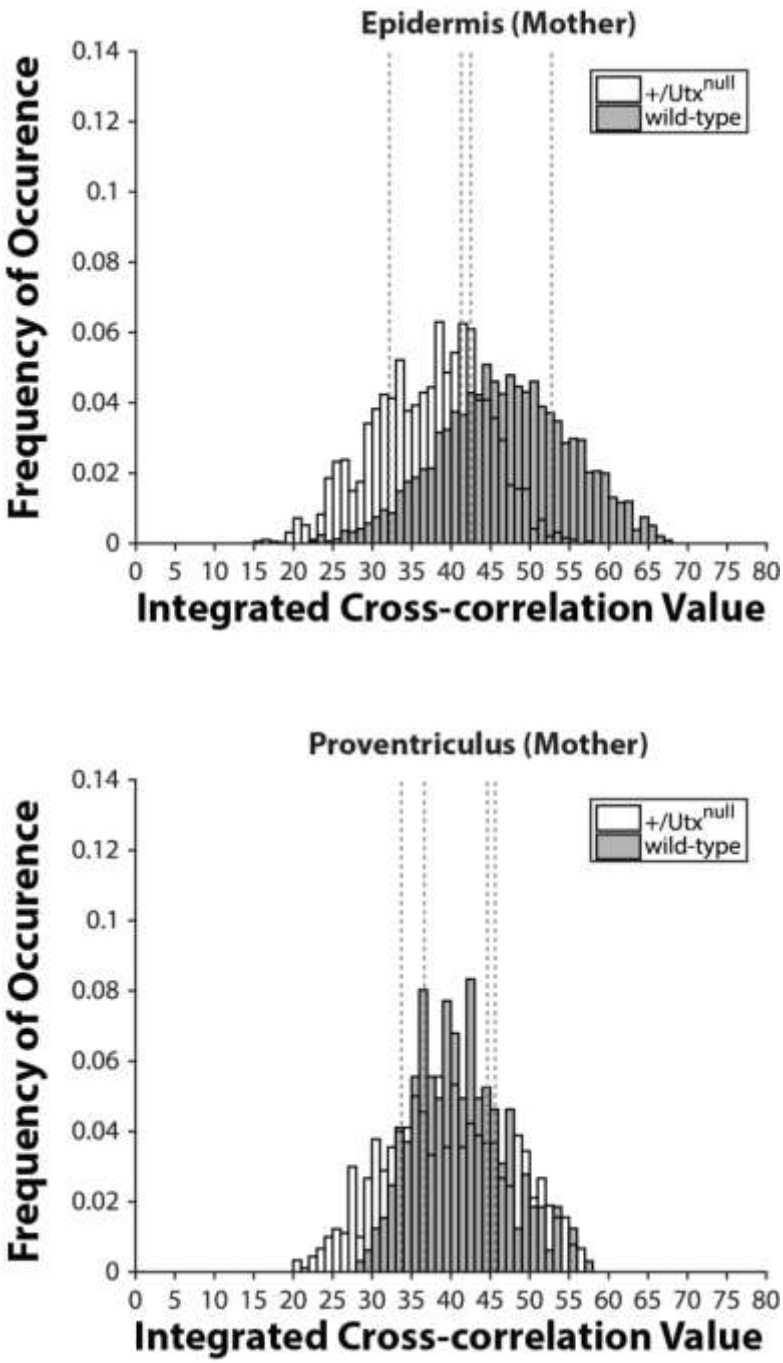

Supplemental Figure S1, The *Utx* mutant does not decrease the correlation of protein synthesis dynamics among cells within a tissue. Cross-correlation of the protein synthesis dynamics between cells within a tissue in transheterozygous wild-type and Utx mutants were performed. Comparisons of the distribution of integrated cross-correlation values showed that more than 50% of data overlap between mutant (n = 44 epidermal cells and 30 proventricular cells) and wild-type animals (n = 58 epidermal cells and 18 proventricular cells). Dashed grey lines denote 1st and 3rd quartiles in the distribution of integrated cross-correlation values.